Applied Surface Science 357 (2015) 1015–1023

Contents lists available at ScienceDirect

Applied Surface Science

journal homepage: www.elsevier.com/locate/apsusc

Comparative temporal analysis of multiwalled carbon nanotube oxidation reactions: Evaluating chemical modifications on true nanotube surface

Flávia G. Pacheco[a], Alexandre A.C. Cotta[a], Honória F. Gorgulho[b], Adelina P. Santos[a], Waldemar A.A. Macedo[a], Clascídia A. Furtado[a,*]

[a] Centro de Desenvolvimento da Tecnologia Nuclear, CDTN/CNEN, CP 941, CEP 31270-901 Belo Horizonte, MG, Brazil
[b] Universidade Federal de São João del Rei, CEP 36300-000 São João del Rei, MG, Brazil

ARTICLE INFO

Article history:
Received 2 June 2015
Received in revised form 31 August 2015
Accepted 5 September 2015
Available online 8 September 2015

Keywords:
Multiwalled carbon nanotubes
Purification
Functionalization
Surface composition
Oxidation debris

ABSTRACT

The influence of extensive purification on oxidized multiwalled carbon nanotube surface composition was studied through the characterization and differentiation of the actual surface submitted to three oxidation methods: microwave-assisted acid oxidation, hydrogen peroxide reflux, and Fenton reaction. The oxidized samples were purified by a multi-step procedure including the sequential use of basic reflux and dispersion in dimethylformamide (DMF). The results showed a significant increase in the amount of oxidation debris with hydrogen peroxide and Fenton reaction times longer than 8 h and strong surface characteristic modification. With regard to sample purification, basic reflux led to a reduction in oxygenated group concentration of only 10% in the samples treated by acid oxidation. On the other hand, the subsequent use of DMF led to a further decrease in concentration of 39%, proving to be a more efficient method for the removal of oxidation debris.

1. Introduction

Oxidation is the functionalization technique most often performed on carbon nanotube (CNT) surface aiming to increase its chemical affinity to various media, enhance dispersion stability and allow further derivatization. This classical chemical route has been broadly used especially to overcome limitations in dispersibility and processability, which are major hindrances in the investigation of their unique properties in applications such as high performance composites and biomedical applications (vaccine development, cancer diagnosis, prevention and treatment, tissue engineering, biosensors, among others). Different oxidation protocols are pointed out in the literature with oxidizers such as HNO_3, HNO_3/H_2SO_4 (mélange solution), H_2SO_4/H_2O_2 (piranha solution), $KMnO_4$, H_2O_2 and Fenton reagent [1–5]. Each method produces materials with different characteristics, varying from the nature and concentration of surface oxygenated groups to their dimensions and structural quality [3,5,6]. Control over these properties is desirable to enhance derivatization yields, improve interactions with matrices and is central for applications in fields such as electronics and biomedicine. Comparisons of oxidation processes and/or oxidation times are common in the literature. However, the purification of the reaction products in those studies was usually performed by neutralization with either basic solutions and/or deionized water [1–3,7,8]. These procedures have been shown to be inefficient in the removal of oxidation debris adhered to CNT surface, which may make up almost a quarter of the sample mass [9]. More recent studies have employed basic solution reflux followed by neutralization to remove oxidation debris through the repulsion created between the negative charge on the CNT surface and the impurities [10–16]. Several studies have investigated changes in nanomaterials due to the application of this protocol. Wang et al. [14], for example, observed that oxidation debris adsorbed onto multiwalled carbon nanotubes (MWCNT) acts as a surfactant and assists stability in aqueous dispersions. Despite the higher reactivity of oxidation debris, Wang et al. [15] showed that oxidized carbon nanotubes still react in a covalent way after purification and perform carbodiimide-promoted amidation. Wu et al. [16] found that exposure of the purified MWCNT surface did not generate significant differences in biological/toxicological effects over human THP-1 cells. Despite the relatively high number of studies on oxidation/purification, the differences between nanotube surfaces regarding the most common oxidation methods in samples submitted to extensive purification are not well

* Corresponding author.
E-mail address: clas@cdtn.br (C.A. Furtado).

http://dx.doi.org/10.1016/j.apsusc.2015.09.054
0169-4332/

established. This paper studied the actual surface characteristics of oxidized MWCNT synthesized by three common oxidation routes: microwave-assisted acid oxidation, hydrogen peroxide reflux, and Fenton reaction. Surface composition differences were analyzed not only due to oxidation method but also time of reaction, assisting in the selection of the best procedure for obtaining oxidized MWCNT to a specific application.

2. Experimental

2.1. Materials

MWCNT was synthesized by chemical vapor decomposition (CVD) of ethylene gas over a 5:5% FeCo catalyst supported on a MgO substrate at 750 °C under argon atmosphere. The pristine material was purified by heat treatment at 400 °C for 30 min, followed by immersion of the solid into 37% HCl overnight. The mixture was filtered and washed with distilled water until neutralization. The sample was further washed with hot water, ethanol and ether. Impurities removal was verified by energy-dispersive X-ray spectroscopy (EDS) and potentiometric titration analysis (Fig. S.1 and Table S.1 of Supporting Information). All reagents and solvents were purchased from Sigma–Aldrich, with the exception of ethanol and ether, which were purchased from Vetec, and used without further purification.

2.2. Oxidation

Three oxidation methods were applied to MWCNT: microwave-assisted acid oxidation, hydrogen peroxide reflux and Fenton reaction.

Microwave-assisted acid oxidation (MA) was performed in duplicate using a START Synth Microwave Synthesis Labstation. 3 g of MWCNT were added to a mixture of HNO_3/H_2SO_4 (1:1) and submitted to 15 heating cycles (500 W) intercalated with 10 s of rest. The mixture was filtered through a 0.45 μm PTFE membrane, neutralized by washing with a pH 10 NaOH solution and deionized water and dried in air at 80 °C overnight. The resulting solid sample was named MAS.

Hydrogen peroxide oxidation (HP) was accomplished by dispersion of 60 mg of MWCNT in 150 mL of a 30% H_2O_2 solution by 20 min bath sonication (135 W). The dispersion was then refluxed at 65 °C for 48 h. 15 mL aliquots were collected at 1, 2, 4, 8, 24 and 32 h. The samples were filtered through a 0.45 μm PTFE membrane, neutralized by washing with pH 10 NaOH and deionized water and dried in air at 80 °C overnight (HPS samples).

Fenton oxidation (FE) was performed through dispersion of 60 mg of MWCNT in a mixture of 112.5 mL of deionized water and 37.5 mL of 30% H_2O_2 by 20 min bath sonication (135 W). 30 mg of Fe_2SO_4 were added to the dispersion and the mixture was magnetically agitated for 48 h. 15 mL aliquots were collected at 1, 2, 4, 8, 24 and 32 h. The samples were filtered through a 0.45 μm PTFE membrane and immersed in 1 M H_2SO_4 overnight. The mixture was filtered through a 0.45 μm PTFE membrane and the solid was neutralized by washing with pH 10 NaOH and deionized water and dried in air at 80 °C overnight (FES samples).

2.3. Purification

All the oxidized samples were purified through a three-step treatment. First, 100 mg of each sample were dispersed in 100 mL of 2 M NaOH by horn sonication for 5 min and refluxed overnight under nitrogen atmosphere. The mixture was filtered through a 0.45 μm PTFE membrane, neutralized by washing with deionized water, and washed with 100 mL of 2 M NaOH and 50 mL of 1 M HCl, followed by neutralization with deionized water after each wash. The samples were further washed with ethanol and dried in air at 80 °C overnight (sample A). After drying, the samples were dispersed in 2 M NaOH by bath sonication for 20 min (135 W) and neutralized and washed as described above. Lastly, the samples were dispersed in N,N-dimethylformamide (DMF) by bath sonication for 1 h (135 W), filtered through a 0.45 μm PTFE membrane and vacuum dried at 150 °C for 3 days (acid oxidation, hydrogen peroxide reflux and Fenton reaction samples named MAP, HPP and FEP, respectively).

2.4. Characterization

Fourier Transform Infrared Spectroscopy (FTIR) measurements were performed in a Thermo Scientific Nicolet spectrometer model Nicolet 6700 with a high sensitivity detector (MCT-A) connected to a Nicolet Centaurus microscope with 10× magnification. FTIR instrument chamber was purged by dry nitrogen in optimal conditions specified by the manufacturer of a 30 scfh flow at 30 psi to avoid air contamination. Raman spectra were collected in a Horiba spectrometer model iHR50 using a 1 mW argon laser (514 nm) with 50× magnification. For both techniques, the samples were prepared by drop coating 0.1 mg/mL pH 12 NaOH dispersion onto a silicon wafer. Different regions of the film were analyzed to verify sample homogeneity. Each sample was prepared and analyzed at least three times each region to assure spectra representation. Baseline correction was realized in all the spectra obtained. Spectra are presented in the same y-scale unless when pointed out. FTIR spectra were subtracted from a background spectrum collected on silicon wafer. Background spectrum was collected before each sample analysis. The influence of NaOH solution on FTIR spectra was analyzed by collecting spectra of pure NaOH film and from one sample after exhaustively rinsing it with deionized water. Results show no significant changes on "O—H" bands as shown by Figs. S.2 and S.3 of Supporting Information.

Transmission electron microscopy (TEM) measurements were performed on a Tecnai G2-12 – SpiritBiotwin FEI microscope operated at 80 kV and on a Tecnai G2-20 – SuperTwin FEI operated at 200 kV. The samples were prepared by drop coating 0.1 mg/mL pH 12 NaOH dispersion onto a 400 mesh holey carbon grid.

Energy-dispersive X-ray spectroscopy (EDS) analysis were performed on a JOEL JXA model 8900RL equipment. Measurements were carried out on pulverized samples deposited on a double-sided tape of carbon in at least three regions of each sample.

XPS measurements were carried out in an ultrahigh vacuum chamber (base pressure lower than 2.0×10^{-10} mbar) using Al Kα X-ray source ($h\nu$ = 1486.68 eV) with a VG Microtech hemispherical electron energy analyzer CLAM 2/1 VU. Samples were prepared by pressing their powder (15 ton) over a KBr pellet. Survey and high-resolution spectra were acquired using 50 eV pass energy. Spectra were analyzed with CasaXPS software.

Potentiometric titration analysis was performed on a Metrohm Titrando 808 apparatus. 10 mg of powder samples were dispersed in a mixture of 99 mL of 0.1 M KCl and 1 mL of 0.1 M HCl. The dispersion was titrated with 0.05 M NaOH in 0.05 M KCl up to pH 11. The result was treated as described by Gorgulho et al. [17].

3. Results and discussion

3.1. FTIR spectroscopy

Figs. 1 and 2 show FTIR spectra of MWCNT samples obtained before and after sample oxidation by microwave-assisted acid reflux (Fig. 1), hydrogen peroxide reflux (Fig. 2a) and Fenton reaction (Fig. 2b). Their analyses indicated that the oxidation reactions were successful, showing multiple vibrational bands related to

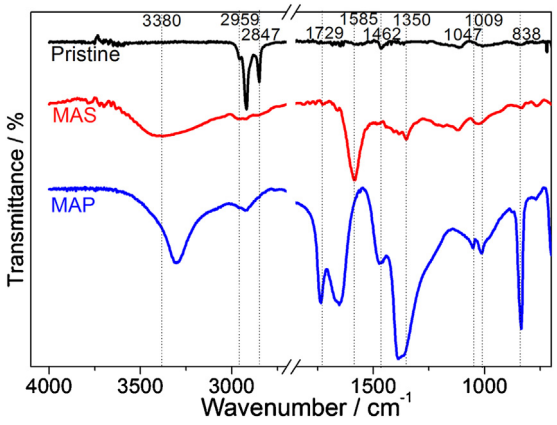

Fig. 1. FTIR spectra of MWCNT oxidized by microwave-assisted acid reflux (MA): pristine (*top*), after oxidation (*middle*) and after oxidation/purification (*bottom*). The intensity of pristine sample spectrum was scaled up by 26 for comparison.

oxygenated functional groups. The absence of a significant carbon nanotube structure vibration bands on pristine sample indicates a high degree of purity and structure integrity of this sample. In a higher amplified spectrum, as shown in Fig. S.4 of Supporting Information, bands at 1500 cm^{-1} and 830 cm^{-1} associated with first order vibrational modes of graphitic structures can also be observed. For comparison with MAS and MAP spectra, pristine sample spectrum was scaled up by 26. Hence, bands associated with "C—H" stretching modes at frequencies of about 2959 (ν(C—H)) and 2847 cm^{-1} (ν(C—H)) became significant. These peaks are however artifacts due to possible hydrocarbon contamination of optical parts of the equipment used [5,18]. Their intensity was low,

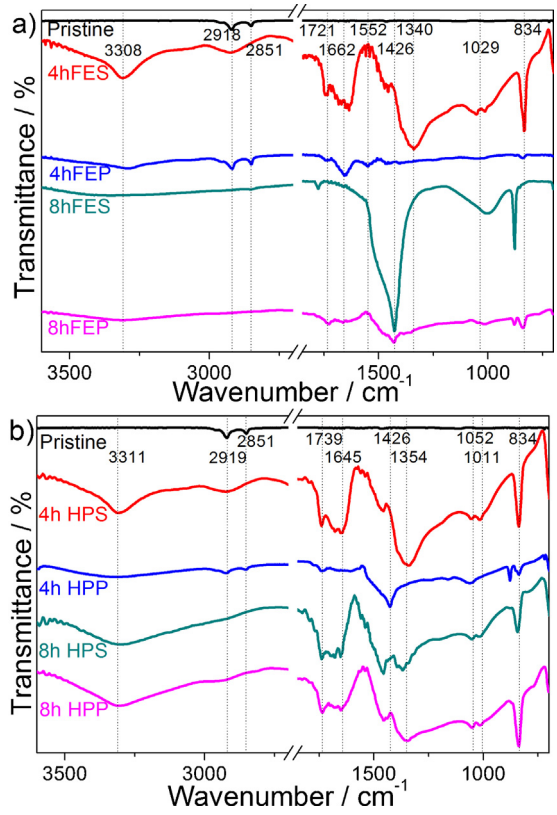

Fig. 2. FTIR spectra of MWCNT oxidized by (a) Fenton (FE) and (b) hydrogen peroxide (HP) reaction: pristine (top), and 4- and 8-h oxidation before (FES and HPS) and after purification (FEP and HPP). The intensity of pristine sample spectrum was scaled up by 26 for comparison.

corresponding to 3% of transmittance variation. The MAS spectrum showed a strong intensification of the vibrational bands related to the carbon nanotube structure at about 1585 cm^{-1} (ν(C=C)). This was expected due to the induction of dipole moments by the creation of defects (insertion of functional groups) [18]. The onset of vibrational bands corresponding to oxygen-containing functional groups was also observed on the MAS spectrum, mainly related to "O—H" stretching and deformation of phenols at 3380 (ν(O—H)) and 1350 cm^{-1} (δ(O—H)) and associated with "C—O" stretching of ethers and alcohols (1047 and 1009 cm^{-1}). Spectra of 4- and 8-h HPS and 4-h FES showed similar results, differing by an increase in the relative intensity of the band at 834 cm^{-1} (τ(C=C)) and the onset of vibrational bands related to the "C=O" stretching of carboxylic acids and aldehydes at 1730 cm^{-1} and of ketones and quinones at 1650 cm^{-1}. These distinctions indicate a higher percentage of acid groups on the surface of these samples when compared to MAS, which is also evidenced by the lower frequency of (ν(O—H)) in these spectra, with a shift from 3380 to 3310 cm^{-1}. In turn, the 8-h FES spectrum presented a higher relative intensity for the bands at 1428 (δ(O—H)) and at 834 cm^{-1} (τ(C=C)) when compared to 1500–1730 cm^{-1} bands and a broader 3310 cm^{-1} band, indicating a higher hydroxyl percentage on the nanostructure surface. The low intensity of 3310 cm^{-1} band is probably related to the use of NaOH solution on the samples preparation, which possible converted a fraction of hydroxyl groups to their salt derivative reducing the intensity of this "O—H" stretching band. Such results evidence a significant difference in chemical environments on the MWCNT surface due to the different oxidation process protocols used.

The FTIR spectra in Figs. 1 and 2 show a deep profile variation due to purification. This result shows the importance of extensive purification to reveal the actual chemical composition of the MWCNT surface. In Fig. 1, the strong presence of carboxylic acids on the MA sample is revealed only after washing its oxidation debris. The strong dipole induction in both functional group and MWCNT bonds increase the intensity of their vibrational modes and evidences an extensive creation of defects on the nanotube surface besides charge transfer between MWCNT and carboxyl groups. Prominent bands at 3300 (ν(O—H)), 1729 (ν(C=O)) and 1350 cm^{-1} (δ(O—H)) in MAP spectrum indicate the stiffening of the hydroxyl and carbonyl bonds and, consequently, the presence of "relatively free" carboxylic acids groups. This stiffening results from the charge transfer from MWCNT to the acceptor carboxylic acid groups. The MWCNT band at 838 cm^{-1} is also pronounced after removal of oxidation debris. For the purified 4-h FE reaction sample, in Fig. 2, a broader band at 3310 cm^{-1} and better resolved bands, especially at 3260 (ν_{COOH}(O—H)), 1721 (ν(C=O)), 1662 (δ(O—H)) and 1552 cm^{-1} (ν(C=C)), were observed. Additionally, there was a significant decrease in the relative intensities of the bands at 1340 and 1426 cm^{-1}. These changes suggest the removal of extensively defected oxidized structures and reveal the presence of remaining carboxylic acids and hydroxyl groups on purified 4-h FE sample. Significant decrease of the relative intensity of the band at 1426 cm^{-1} (δ(O—H)) and a downshift of the bands related to carboxyl and structural carbon nanotube vibrations were observed for the 8-h FE sample after purification. The 8-h FEP spectrum showed also the presence of higher relative intensity bands associated with ν(C=O) and δ(O—H) vibrations of carboxylic acids (1721 and 1662 cm^{-1}, respectively) and a shift from 3335 to 3308 cm^{-1} of the peak position of ν(O—H) band. The HP oxidation spectra, on the other hand, showed 4- and 8-h purified sample profiles (HPP) more similar to those of 8- and 4-h post-synthesis (HPS) profiles, respectively. According to the relative intensities of hydroxyl/carbonyl bands of 4-h HP spectra, the purified 4-h HP oxidation sample seemed to be richer in hydroxyls than their oxidation debris. The 8-h HP, in turn, does not present a significant difference on hydroxyl/carbonyl intensity bands. The presence of

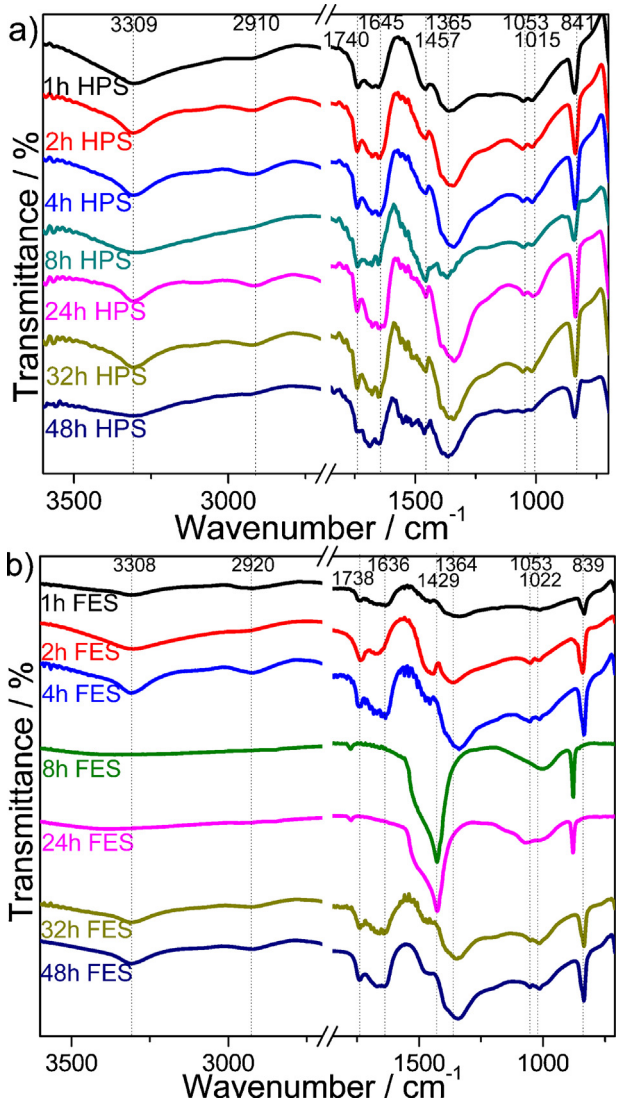

Fig. 3. FTIR spectra of post-synthesis MWCNT oxidized by (a) hydrogen peroxide (HP) and (b) Fenton reaction (FE).

carboxylic acid groups is maintained after purification (8-h HPP spectrum).

The temporal evolution of the FTIR spectra of FE and HP oxidation of MWCNT samples can be seen in Fig. 3. From their analysis, it is possible to observe variations in the hydroxyl/carbonyl relative intensity and frequency of the vibrational bands over time, with the most significant changes in the 8-h samples. The HP and FE reactions are pointed out to occur via the attack of hydroxyl radicals on the defective sites (firstly) and unsaturated bonds (secondly) of the carbon nanostructure, with the consequent generation of phenols [18,19]. With the progress of the oxidation process, phenols were converted into carbonyl and carboxylic acids. Such changes appear to be evident in the spectra shown in Fig. 3. For short oxidation times, the FTIR spectra showed the progress of the reaction with the preferential formation of carbonyl bands, represented by the narrowing and slightly downshift of the band around 3310 cm^{-1} and the increase on the relative intensity of their bands (1640–1740 cm^{-1}) compared to the 3310 cm^{-1} one. This advancement, however, is limited due to the complete functionalization of pristine defective sites and edges and the beginning of the attack on the MWCNT carbonic structure, which leads to the generation of new defects and may subsequently break the carbonic structure. These newly formed defects and oxidation residues are preferentially oxidized turning the surface richer in hydroxyl groups again. Such behavior is in accordance with a cyclic mechanism as discussed by Li et al. [19] and Peng and Liu [20] that may lead to the degradation of the structure with tube shortening and ring opening in a very prolonged oxidation time. The increase in the percentage of hydroxyl groups can also be attributed to the fact that carboxylic acids are strong electron acceptors, attracting the electrons of the resonant ring and converting themselves into diols, since the reaction proceeds in an acidic environment. These processes lead to a broadening of the band associated with ν(O—H) (around 3310 cm^{-1}) and its shift to higher frequencies, as well as the reduction in the relative intensity related to carbonyl stretching bands as observed for the 8-h reaction time. The relative frequencies of the vibrations of the carbonic structure (~1500 and 840 cm^{-1}) are slightly increased and intensified due to the induction of the dipole moment from the creation of new defects and the more significant presence of a group that is a strong electron donator to the aromatic ring (hydroxyls). With the advancement of the oxidative process, however, the hydroxyls formed are converted into carbonyls and carboxyls, which leads to a weakening of the bonds between the carbon atoms and the consequent reduction in their vibration frequency [5]. Bands related to the stretching vibrations of the carboxylic acid groups were also intensified, leading the spectrum aspect to return to that of a short reaction time.

The comparison to the spectra in Fig. 3 with those for the 4- and 8-h purified samples (Fig. 2) suggests that the HP oxidation cycle restarted in less than 4 h, since the latter indicates a more significant increase in the relative percentage of hydroxyl groups on the MWCNT surface than on its oxidation debris. This result indicates that the attack on the graphitic structure had already occurred to a significant extent, producing more hydroxyls. The 4-h FEP reaction spectra, on the other hand, showed more intense carboxyl group bands than for 8-h FEP, but less intense than for 4-h FES. Therefore, its oxidation cycle seemed to restart between 4 and 8 h. These results show that the HP oxidation route was more aggressive and attacked the MWCNT aromatic structure in a shorter oxidation time when compared to FE reaction.

3.2. Raman spectroscopy

The temporal analysis of the HP and FE reactions was also performed by Raman spectroscopy. The Raman spectrum of carbon nanotubes in the 1000–2000 cm^{-1} region presents two strong characteristics bands at frequencies of about 1360 cm^{-1} ("D" band) and 1580 cm^{-1} ("G" band). The "D" band represents the relaxation mode of the benzene ring due to the presence of defects and is therefore related to the presence of amorphous and disordered carbon atoms. The "G" band, in turn, originates from in-plane tangential stretching of carbon bonds of the graphitic structure with E_{2g} symmetry [21]. The intensity ratio of these bands (I_D/I_G) reflects an increase in defect density. Raman spectra of pristine MWCNT sample and MAP sample are presented in Fig. S.5 of Supporting Information. The variation in the intensity ratio of bands "D" and "G" as a function of time is displayed in Fig. 4. In this figure we can observe a trend of an initial increase in the structural quality, represented by a decrease in the "D/G" band intensity ratio, followed by its decrease with the reaction duration. This behavior was also observed by Peng and Liu [20] and can be attributed to the fact that oxidation initially leads to the consumption of the remaining oxidation debris and disordered regions of the sample due to their greater reactivity, resulting in an increase in structural quality. The subsequent decline was due to an attack to the carbon structure and the consequent generation of new defects and new edges on the surface of the tubes. Defect generation started to become greater than the consumption of the disordered regions with reaction times of 8 and 24 h for HP and

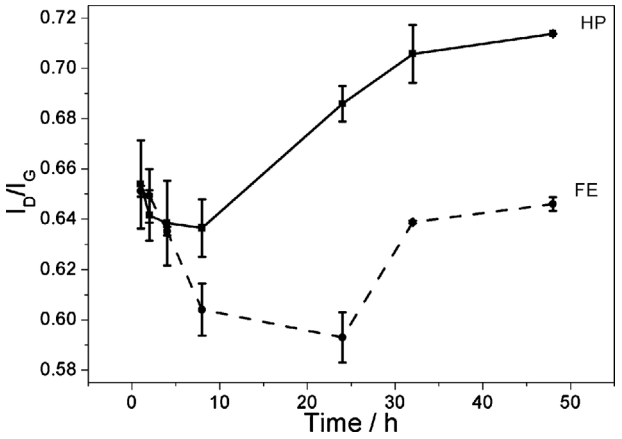

Fig. 4. I_D/I_G ratio variation in Raman spectra of MWCNT oxidized by hydrogen peroxide (HP) and Fenton reaction (FE) before the purification step.

FE oxidations, respectively. Such variation suggests again that the HP reaction kinetics is faster, allowing it to damage more MWCNT under the study conditions.

The Raman "D/G" band intensity ratio of purified samples is shown in Table 1. The values are averages of at least seven spectra of different regions for each sample. All the obtained spectra of MAP sample are presented in Fig. S.6 of Supporting Information, as an example. These results seem to indicate that MA oxidation was more aggressive to MWCNT surface when compared to 4- and 8-h HP and FE samples. This result corroborates to the strong dipole induction in MAP sample characterized by FTIR. The 4-h FEP sample seemed to present a slightly higher structural quality than the 8-h sample. The opposite behavior was observed for HPP samples. The variation of structural quality with purification was expected due to the removal of oxidation debris on purified samples. As previously mentioned oxidation of MWCNT structure start with the attack of hydroxyl radical to MWCNT unsaturated bonds with consequent insertion of hydroxyl groups. These groups are further oxidized forming carboxyl groups. With the advancement of oxidation reaction, the carbon structure would cut the samples with consequent generation of shorter tubes and debris, which are more oxidized/defective than the nanotube. At this point the sample presents a better structural quality than in the previous step

Table 1
I_D/I_G ratios of purified oxidized samples obtained from Raman spectra.

Sample	I_D/I_G
MWCNT	0.607 ± 0.005
MA	0.810 ± 0.008
4-h FE	0.595 ± 0.005
8-h FE	0.605 ± 0.011
4-h HP	0.624 ± 0.010
8-h HP	0.600 ± 0.013

Table 2
Percentage composition (% at) of samples according to XPS analysis.

Sample	O	C
MWCNT	1.3	98.7
MAS	7.9	92.1
MAP	4.9	95.1
4-h FES	10.3	89.7
4-h FEP	2.9	97.1
8-h FES	7.9	92.1
8-h FEP	3.2	96.8
4-h HPS	4.4	95.6
4-h HPP	3.4	96.6
8-h HPS	7.7	92.3
8-h HPP	7.3	92.7

of the cycle, since a fraction of its defects were removed as oxidation debris. Thus, a lower I_D/I_G ratio is presented by the purified sample when compared to the not purified sample. These results suggest that the oxidation cycle restarted before and after 8 h for the HP and FE reactions, respectively. Given the results of the analyses by FTIR and Raman spectroscopy, the reaction times of 4 and 8 h seem to be optimal for HP and FE oxidations, respectively, when the preservation of the structural quality and a significant presence of functional groups on MWCNT surface are considered.

3.3. XPS analysis

XPS results indicate only carbon and oxygen elements are present on samples surface in a significant concentration. XPS survey spectra for pristine and MAS samples are presented in Fig. S.7 of Supporting Information. Carbon and oxygen percentage composition of all samples components are presented in Table 2. These results show that post-synthesis samples contain higher oxygen content as expected due to removal of highly oxidized debris with purification. MA sample, for example, presented a significant

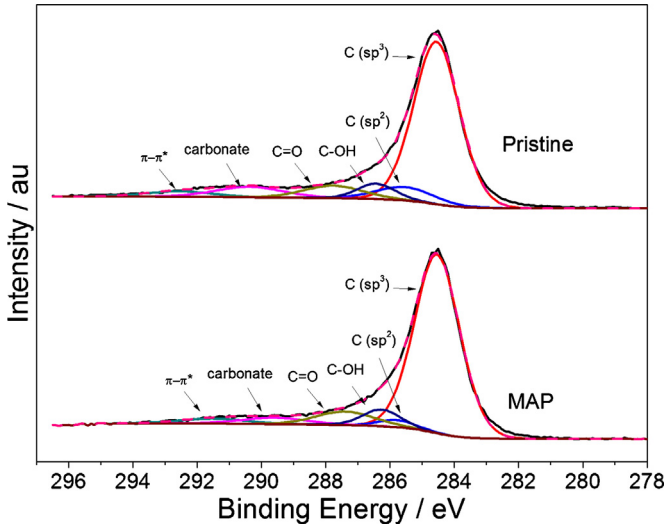

Fig. 5. High resolution deconvoluted peaks of XPS C1s spectra from pristine and MAP sample.

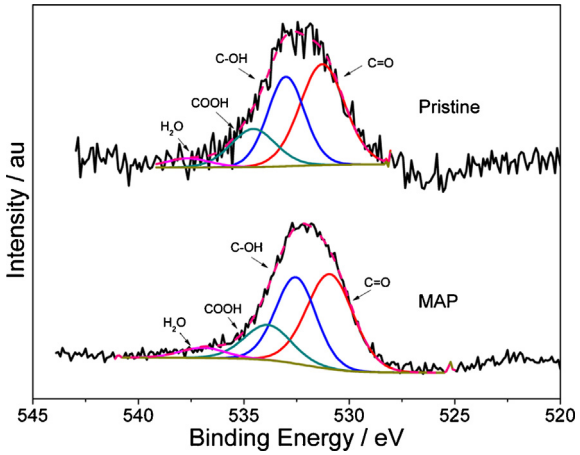

Fig. 6. High resolution deconvoluted peaks of XPS O1s spectra from pristine and MAP sample.

removal of oxygenated groups due to the purification of about 50% when considering only the carbon and oxygen atoms of samples (excluding adsorbed water and carbonates), with an oxygen reduction of 8.32–4.59 from MAS to MAP sample. It can also be observed on purified samples that longer times of oxidation have produced samples with higher oxygen levels. 4-h FES sample, however, presented a higher oxygen percentage than 8-h FES sample. This result indicates a significant fraction of the debris generated in the first 4 h of reaction were consumed in the subsequent 4 h, which occurred concomitant to nanotube oxidation, once 8-h FEP presents a higher oxygen content than 4-h FEP. 4-h HPS sample, in turn, presented lower oxygen content than the 8-h FES one. These results suggest again that FE and HP reactions present different kinetics. Based on previous results it seems most of the debris generated in the first hours of HP reaction were consumed before 4 h of reaction.

XPS C1s spectra were resolved in six peaks related to carbon atoms in graphitic structure at 284.5 eV, aliphatic structures, edges and defects in graphitic structure at 285.4 eV, phenolic, alcohol and ether groups at 286.5 eV, carbonyl, quinone, carboxyl and lactone at 287.8 eV, carbonates groups associated to adsorbed CO_2 molecules from 289 to 291 eV and satellite peaks due to π–π^* transitions from 291 to 294 eV [6]. XPS O1s spectra was resolved in five peaks related to carbonyl oxygen atoms in carbonyl, quinone, carboxyl and lactone groups at 531.1 eV, oxygen atoms in hydroxyls and ethers at 532.0 eV, carboxylic acids at 533.6 eV, adsorbed water from 535 to 537 eV and metal oxides from 528 to 531 eV [6]. As an example, the C1s and O1s deconvoluted peaks of pristine and MAS samples spectra are shown in Figs. 5 and 6. Carbonyl, hydroxyl and carboxyl concentrations calculated by O1s peak deconvolution for

Table 3
Percentage composition (% at) of samples according to XPS O1s analysis when considering just hydroxyl, carbonyl and carboxyl oxygenated groups.

Sample	Binding energy (eV)		
	530.8–531.9 C═O (%)	532.4–533 C—OH (%)	533.9–535 COOH (%)
MWCNT	47.4	34.6	18.0
MAS	50.5	42.5	7.0
MAP	46.3	36.6	17.1
4-h FES	55.2	39.9	4.9
4-h FEP	34.6	44.8	20.6
8-h FES	38.7	57.0	4.3
8-h FEP	26.1	56.7	17.2
4-h HPS	37.1	36.8	26.1
4-h HPP	33.3	50.9	15.8
8-h HPS	11.1	54.5	34.4
8-h HPP	24.4	40.7	34.9

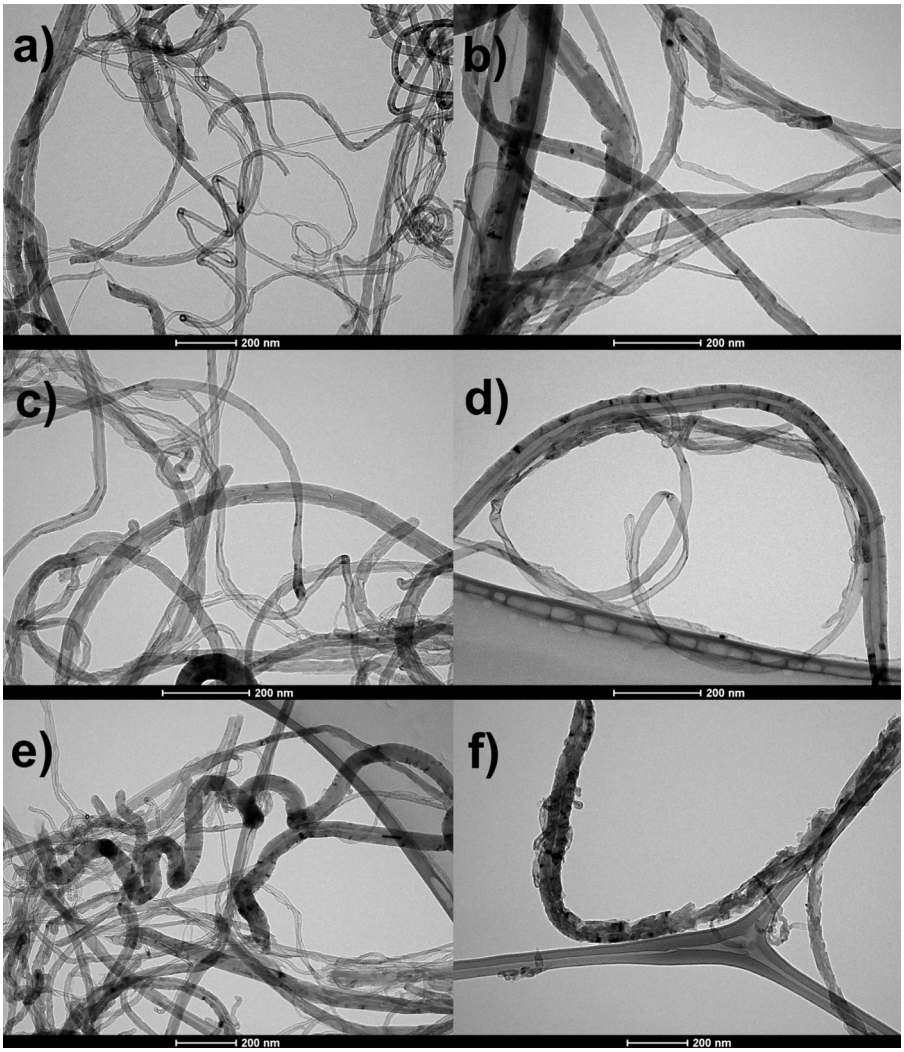

Fig. 7. TEM images of raw MWCNT (a) and purified MWCNT oxidized by acid reflux (b), Fenton reaction for 8 h (c), 48 h (d) and hydrogen peroxide reaction for 8 h (e) and 48 h (f).

all samples is summarized in Table 3. These results agree with FTIR results discussed. For FE reaction, for example, it is observed a higher percentage of hydroxyl groups on the surface of 8-h FES and 4-h FEP samples when compared to 8-h FEP and 4-h FES, respectively. When analyzing HP reaction results, in turn, higher percentages of hydroxyl groups are observed for 4-h HPP and 8-h HPS samples when compared to 4-h HPS and 8-h HPP, respectively. These results show the introduction of mainly hydroxyl groups on the MWCNT surface when compared to carbolxylic acid groups through HP and FE reactions and suggest again the HP oxidation route present a faster kinetic than FE reaction.

Table 4
Oxygenated group concentrations (mmol/g) over oxidized MWCNT samples by potentiometric titration.

Sample	Carboxylic acid	Lactone	Phenol	Total
MAS	0.59	0.63	26.82	28.0
MA (Sample A)	0.82	–	24.39	25.2
MAP	0.34	0.13	13.94	14.4
4-h FEP	0.19	0.03	1.96	2.2
8-h FEP	0.11	0.14	9.91	10.2
4-h HPP	0.26	0.20	8.02	8.5
8-h HPP	0.35	0.02	16.37	16.7

3.4. Titration analysis

Potentiometric titration analysis showed a significant reduction in the total concentration of oxygenated groups due to purification, as shown in Table 4. In this work, the functional groups were identified according to their pK_a values. Carboxylic acids present low pK_a values, below 7.0. Phenolic groups, in turn, present relatively high pK_a values, which usually correspond to values between 9.0 and 11.0. Intermediate pK_a values are associated with other groups, such as lactones. The limits were adapted from Gorgulho et al. [17] taking into account the FTIR results presented. Both potentiometric titration and XPS results show the significant removal of oxygenated groups due to purification of about 50% for MA sample, which is associated to a 10% mass reduction. This result shows that oxidation debris are much richer in oxidized groups. It also indicates the importance of a more extensive purification of the oxidized samples, since almost 40% from the 50% oxygenated groups' removal is related with the purification steps performed after basic reflux. Potentiometric titration and XPS results also agree that 8-h HPP is the most oxidized purified sample, proving HP to be the most effective oxidation route for the conditions studied. All purified samples presented high concentrations of phenolic groups, regardless of the oxidation method employed. This result conflicts with potentiometric titration data. This difference is probably related to these techniques limitations. Titration requires long stabilization times and analyzes only exposed surface groups. This way it may fail in quantifying samples with large amounts of oxygenated groups and/or with not completely dispersed samples. XPS, in turn, estimates the composition of only of the uppermost layers. This result suggests that carboxylic acid groups tend to aggregate more effectively becoming less exposed. HP samples were

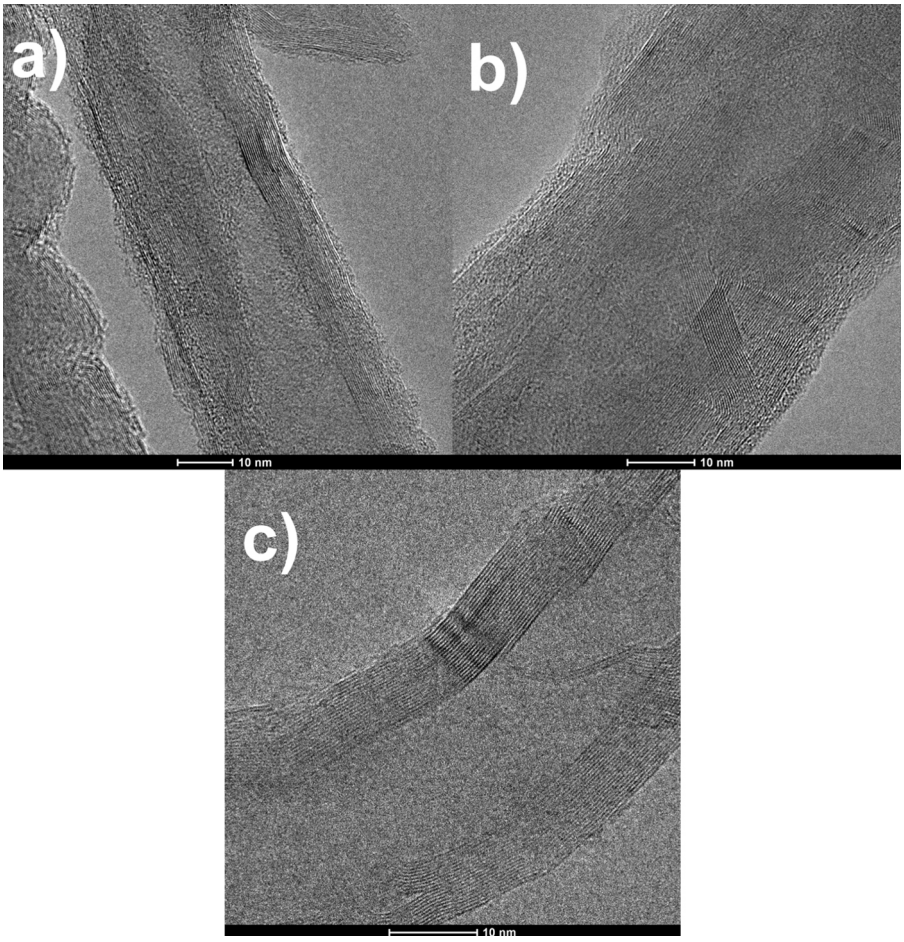

Fig. 8. TEM images of MWCNT oxidized by acid reflux (a) synthesized (MAS), (b) after basic sonication and (c) after DMF sonication.

richer in oxygenated groups than FE samples, indicating HP to be a more aggressive reaction, once again, under the conditions used.

3.5. Electron microscopy

Low-magnification TEM images suggests a similar apparent structural quality for all samples except the one obtained with a long HP oxidation time (48 h), which strongly damaged MWCNT surface (Fig. 7). This result is in accordance with the aggressive condition pointed out by the other analyses and shows that the oxidation process is highly dependent on both the reactants and the reaction time, allowing the HP oxidation to damage the nanomaterial surface more than the acid treatment. Similar observations were made by Yang et al. [8], who reported higher I_D/I_G ratio and oxygen-containing functional group concentration for 12-h HP reflux when compared to 4-h acid reflux (HNO_3/H_2SO_4).

With regard to the purification protocol adopted in this work, the use of a second basic treatment (sonication in basic medium) and DMF after a basic reflux treatment led to further removal of 17% and 22% of the total mass removed from the MAS sample, respectively. Such improvement is probably due to the use of ultrasound force, which is capable of peeling off not only the charged debris, but also other particles adhered to the MWCNT surface, and to an efficient stabilization of these impurities by DMF, which allowed their extraction by a filtration step. High-resolution TEM images of purified samples showed the removal of a layer of amorphous material adsorbed on the surface, as exhibited in Fig. 8. In these images, we can observe the presence of a partially amorphous material involving the nanotubes (Fig. 8a), which may be attributed to adsorbed oxidation debris. The basic treatments charge the debris and allow them to be peeled off by ultrasonic power. However, sodium bicarbonate is probably generated through the contact of the basic solution with air and lumps up on nanotube surface (Fig. 8b). Impurities virtually disappeared with the final treatment with DMF (Fig. 8c), probably by dissolution of the remaining impurities by the solvent. The final sample barely presented any material deposited on its surface, indicating the good efficiency of the adopted procedure.

4. Conclusions

This work demonstrated that the application of an extensive purification procedure to oxidized MWCNT leads to deep modifications of the MWCNT surface chemical composition, regardless of the oxidation route adopted. Analysis of the actual MWCNT surfaces obtained with the three oxidation methods showed that both reactant and reaction time might affect MWCNT properties profoundly, such as long period hydrogen peroxide oxidation, which may cause more damage to MWCNT than acid reflux under the studied conditions. It was also observed that the oxidation debris is much richer in oxidized groups than the MWCNT and that its removal leads to a reduction of almost 50% in the total oxidized group concentration in the sample. Literature proposed cyclic oxidation mechanisms for HP and FE reactions could further be followed by FTIR spectra with clear variations in relative hydroxyl/carbonyl presence on MWCNT and oxidation debris. These results show that more accurate purification is required for a more controlled manipulation of MWCNT and a more precise determination of quantities and characteristics of the samples. With regard to sample purification, it was observed that the use of multiple steps after basic reflux significantly decreased the remaining debris, thus improving purity and allowing a more appropriate application in different fields.

Acknowledgments

This work was supported by the Brazilian Nanocarbon Institute, the Brazilian Nanomat Network (Fapemig process number CEX – RDP-00116-10), the Brazilian Network on Nanotoxicology (CNPq process number 552131/2011-3), Brazilian agencies CNPq, CAPES, FAPEMIG, CNEN and Vale S.A. The authors acknowledge the Nanomaterials Laboratory of the Physics Department of the Federal University of Minas Gerais, especially Sérgio de Oliveira and Luiz Orlando Ladeira, for providing MWCNT samples and access to the microwave reactor, Anderson Oliveira (UFSJ) for his advice on potentiometric titration analysis and Roberto Luiz Moreira (UFMG), Ester Figueiredo de Oliveira, João Paulo Coelho and Jefferson Patrício Nascimento (CDTN) for assistance in infrared and Raman spectroscopy.

Appendix A. Supplementary data

Supplementary data associated with this article can be found, in the online version, at http://dx.doi.org/10.1016/j.apsusc.2015.09.054.

References

[1] J. Chen, Q. Chen, Q. Ma, Influence of surface functionalization via chemical oxidation on the properties of carbon nanotubes, J. Colloid Interface Sci. 370 (2012) 32–38.
[2] Y.-C. Chiang, W.-H. Lin, Y.-C. Chang, The influence of treatment duration on multi-walled carbon nanotubes functionalized by H_2SO_4/HNO_3 oxidation, Appl. Surf. Sci. 257 (2011) 2401–2410.
[3] I. Mazov, V.L. Kuznetsov, I.A. Simonova, A.I. Stadnichenko, A.V. Ishchenko, A.I. Romanenko, E.N. Evgeniy, O.B. Anikeeva, Oxidation behavior of multiwall carbon nanotubes with different diameters and morphology, Appl. Surf. Sci. 258 (2012) 6272–6280.
[4] L. Zhang, V.U. Kiny, H. Peng, J. Zhu, R.F.M. Lobo, J.L. Margrave, V.N. Khabashesku, Sidewall functionalization of single-walled carbon nanotubes with hydroxyl group-terminated moieties, Chem. Mater. 16 (2004) 2055–2061.
[5] U.J. Kim, C.A. Furtado, X. Liu, G. Chen, P.C. Eklund, Raman and IR spectroscopy of chemically processed single-walled carbon nanotubes, J. Am. Chem. Soc. 127 (2005) 15437–15445.
[6] V. Datsyuk, M. Kalyva, K. Papagelis, J. Parthenios, D. Tasis, A. Siokou, I. Kallitsis, C. Galiotis, Chemical oxidation of multiwalled carbon nanotubes, Carbon 46 (2008) 833–840.
[7] R.H. Bradley, K. Cassity, R. Andrews, M. Meier, S. Osbeck, A. Andreu, C. Johnston, A. Crossley, Surface studies of hydroxylated multi-wall carbon nanotubes, Appl. Surf. Sci. 258 (2012) 4835–4843.
[8] S. Yang, X. Wang, H. Yang, Y. Sun, Y. Liu, Influence of the different oxidation treatment on the performance of multi-walled carbon nanotubes in the catalytic wet air oxidation of phenol, J. Hazard. Mater. 233–234 (2012) 18–24.
[9] S. Fogden, R. Verdejo, B. Cottam, M. Shaffer, Purification of single walled carbon nanotubes: the problem with oxidation debris, Chem. Phys. Lett. 460 (2008) 162–167.
[10] K. Flavin, I. Kopf, E. Del Canto, C. Navio, C. Bittencourt, S. Giordani, Controlled carboxylic acid introduction: a route to highly purified oxidised single-walled carbon nanotubes, J. Mater. Chem. 21 (2011) 17881–17887.
[11] E. Del Canto, K. Flavin, D. Movia, C. Navio, C. Bittencourt, S. Giordani, Critical investigation of defect site functionalization on single-walled carbon nanotubes, Chem. Mater. 23 (2011) 67–74.
[12] C.G. Salzmann, S.A. Llewellyn, G. Tobias, M.A.H. Ward, Y. Huh, M.H.L. Green, The role of carboxylated carbonaceous fragments in the functionalization and spectroscopy of single-walled carbon-nanotube material, Adv. Mater. 19 (2007) 883–887.
[13] R. Verdejo, S. Lamoriniere, B. Cottam, A. Bismarck, M. Shaffer, Removal of oxidation debris from multi-walled carbon nanotubes, Chem. Commun. 5 (2007) 513–515.
[14] Z. Wang, M.D. Shirley, S.T. Meikle, R.L.D. Whitby, S.V. Mikhalovsky, The surface acidity of acid oxidised multi-walled carbon nanotubes and the influence of in-situ generated fulvic acids on their stability in aqueous dispersions, Carbon 47 (2009) 73–79.
[15] Z. Wang, A. Korobeinyk, R.L.D. Whitby, S.T. Meikle, S.V. Mikhalovsky, S.F.A. Acquah, H.W. Kroto, Direct confirmation that carbon nanotubes still react covalently after removal of acid-oxidative lattice fragments, Carbon 48 (2010) 916–918.
[16] Z. Wu, R.F. Hamilton, Z. Wang, A. Holian, S. Mitra, Oxidation debris in microwave functionalized carbon nanotubes: chemical and biological effects, Carbon 68 (2014) 678–686.

[17] H.F. Gorgulho, J.P. Mesquita, F. Gonçalves, M.F.R. Pereira, J.L. Figueiredo, Characterization of the surface chemistry of carbon materials by potentiometric titrations and temperature-programmed desorption, Carbon 46 (2008) 1544–1555.
[18] U.J. Kim, X.M. Liu, C.A. Furtado, G. Chen, R. Saito, J. Jiang, M.S. Dresselhaus, P.C. Eklund, Infrared-active vibrational modes of single-walled carbon nanotubes, Phys. Rev. Lett. 95 (2005) 157402.
[19] W. Li, Y. Bai, Y. Zhang, M. Sun, R. Cheng, X. Xu, Y. Chen, Y. Mo, Effect of hydroxyl radical on the structure of multi-walled carbon nanotubes, Synth. Met. 155 (2005) 509–515.
[20] Y. Peng, H. Liu, Effects of oxidation by hydrogen peroxide on the structures of multiwalled carbon nanotubes, Ind. Eng. Chem. Res. 45 (2006) 6483–6488.
[21] M.S. Dresselhaus, G. Dresselhaus, R. Saito, A. Jorio, Raman spectroscopy of carbon nanotubes, Phys. Rep. 409 (2005) 47–99.